JGR Earth Surface

RESEARCH ARTICLE
10.1029/2022JF006820

Influence of Sand Supply and Grain Size on Equilibrium Upper Regime Bedforms

Sydney Sanders[1], Sadegh Jafarinik[1,2], Ricardo Hernandez Moreira[1,3], Ryan Johnson[1], Amanda Balkus[1], Mahsa Ahmadpoor[1], Brandon Fryson[1], Briana McQueen[1], Juan Fedele[4], and Enrica Viparelli[1]

[1]Department of Civil and Environmental Engineering, University of South Carolina, Columbia, SC, USA, [2]Arcadis U.S., Inc., Columbus, OH, USA, [3]Hanson-Rodríguez SRL, Santo Domingo, Dominican Republic, [4]Exxon Mobil Upstream Research Company, Houston, TX, USA

Key Points:

- The ratio of volume transport of sediment to volume transport of water Q_s/Q_w plays a prime control on equilibrium bed configuration
- The length of upstream migrating bedforms increases with the ratio between sediment supply and flow discharge
- The presence of suspended bed material load seems to favor the formation of upstream migrating bedforms

Supporting Information:

Supporting Information may be found in the online version of this article.

Correspondence to:

E. Viparelli,
viparell@cec.sc.edu

Citation:

Sanders, S., Jafarinik, S., Hernandez Moreira, R., Johnson, R., Balkus, A., Ahmadpoor, M., et al. (2023). Influence of sand supply and grain size on equilibrium upper regime bedforms. *Journal of Geophysical Research: Earth Surface*, *128*, e2022JF006820. https://doi.org/10.1029/2022JF006820

Received 4 JUL 2022
Accepted 5 JUL 2023

Abstract

Notwithstanding the large number of studies on bedforms such as dunes and antidunes, predicting equilibrium bedform type and geometry for a given flow regime, sediment supply and caliber remains an open problem. Here, we present results from laboratory experiments specifically designed to study how upper regime bedform type and geometry vary with sediment supply and caliber. Experiments were performed in a sediment feed flume with flow rates varying between 5 and 30 l/s and sand supply rates varying between 0.6 and 20 kg/min. We used both uniform and non-uniform sands with geometric mean diameters varying between 0.22 and 0.87 mm. Analysis of our data and data available in the literature reveals that the ratio of total (bedload plus suspension) volume transport rate of sediment to water discharge Q_s/Q_w plays a prime control on upper regime equilibrium beds. Equilibrium bedforms transition from washed out dunes (lower regime) to downstream migrating antidunes (upper regime) for Q_s/Q_w between 0.0003 and 0.0007. For values of Q_s/Q_w greater than 0.0015, the bedform length increases with Q_s/Q_w. At these high values of Q_s/Q_w, equilibrium in fine sand is characterized by upstream migrating antidunes, cyclic steps, and significant suspended load. In experiments with coarse sand, equilibrium is characterized by plane bed with bedload transport in sheet flow mode. Standing waves form at the transition between downstream migrating antidunes and upstream migrating bedforms.

Plain Language Summary

Bedforms are sediment bumps that form and move at the bottom of channels transporting water and sediment. Bump size and direction of movement depend on flow and sediment properties. Although bedforms have been observed and studied for a long time, predicting type and shape remains to be open problems. Here, we present results from laboratory experiments designed to study bedforms made of sand that form under fast flows. Our results show that, in these conditions, bedform type and size depend on the ratio between volumes of transported sediment and water and the size of sand grains. In addition, our results suggest that if sand is transported in a thin layer near the bed, bedforms tend to move in the direction of the flow, while bedforms tend to move in the direction opposite to the flow if some sand is suspended in the water column.

1. Introduction

The interaction between flowing water and a mobile bed composed of loose sediment often results in bedform formation in both shallow (fluvial, coastal, and glacigenic) and deep-water settings (Alexander et al., 2001; Araya & Masuda, 2001; Best, 2005; Covault et al., 2017; Froude et al., 2017; Kostaschuk et al., 2010; Lang et al., 2021; Paola et al., 1989; Parkash and Middleton, 1970; Spinewine et al., 2009). Subaerial (fluvial, open channel, and shallow water) bedforms are generally divided into two broad categories: those with height and length that scale with flow depth (small bedforms) and bedforms with height and length that scale with flow depth and channel width (bars), respectively (Garcia, 2008; Hayashi & Ozaki, 1979; Ikeda, 1984; Seminara, 2010). Open channel small bedforms are further classified into lower and upper regimes, loosely linked to specific hydraulic states of the flow (e.g., Froude number). Lower regime bedforms are out of phase with the bed surface (e.g., dunes) and are generally associated with relatively high flow resistance due to flow separation. Upper regime bedforms, on the contrary, are typically in phase with water surface oscillations, presenting in some cases little or no flow separation (Simons and Richardson, 1962, 1966; Task force on Bedforms in Alluvial Channels, 1966). The

extrapolation of these long-standing definitions to deep-water (subaqueous) cases has been recently challenged in light of new experimental and some field data (Fedele et al., 2016).

Bedform phase diagrams and relations based on empirical data or mathematical modeling abound and were proposed to determine equilibrium bedform type and geometry in terms of non-dimensional parameters representative of flow and sediment properties (see e.g., Andreotti et al., 2012; Charru et al., 2013; Colombini, 2004; Colombini & Stocchino, 2008; Engelund, 1970; Garcia, 2008; Ohata et al., 2017, 2022; Pen et al., 2018; Simons and Richardson, 1966; Southard and Boguchwal, 1990; Vanoni, 1974; Yokokawa et al., 2011). Incorporating these criteria into morphodynamic models, however, remains a challenge because given the hydrologic regime, sediment supply and caliber, a resistance formulation is needed to characterize the flow. Flow resistance, bed roughness and friction factors in the presence of bedforms may be very different than in the case of a flat, granular bed (Einstein & Barbarossa, 1952). Estimating flow properties using existing bedform predictors is thus challenging because flow resistance is not properly estimated when the bed configuration is unknown (van Rijn, 1984).

We present experimental results on the open channel, upper regime bedforms at equilibrium, that is, when bed elevation averaged over a series of bedforms does not change in time. The scope of the experiments was to understand if and how antidune geometry and migration direction varied with the sand supply rate, grain size, and preferential mode of transport, such as bedload or suspended load. In other words, experiments were designed to investigate if upper regime bedforms at equilibrium depend on parameters controlling the equilibrium state, that is, flow regime, sediment supply and caliber (Blom et al., 2016, 2017; Seminara, 2010; Viparelli and Eke, 2021).

This paper is organized as follows: we briefly discuss previous research on bedform progression relevant to this study and then present an overview of the experimental program followed by a description of the experimental setup and procedures. Experimental results are then presented, and our results are compared with previous open channel flow and submarine experiments in the discussion section.

2. Bedform Progression in Open Channels Transporting Sand

Bedform progression is well understood in fine sands, defined here as sands with characteristic grain size smaller than 0.5 mm (Garcia, 2008). If we consider a laboratory flume with a plane bed of uniform fine sand and consider to gradually increase flow velocity, we first observe water flowing on an immobile bed, then sediment grains start moving and ripples form. As flow velocity further increases, bedforms evolve into dunes, which migrate downstream. In the presence of well-developed dunes, the water surface is low on crests and high on troughs. At relatively high velocities dunes are washed out and the bed becomes flat again. This flat bed at the transition between dunes and antidunes is called the *upper regime plane bed* and sediment transport is characterized by individual grains rolling "*almost continuously downstream in sheets one or two grain diameters thick*" (Simons and Richardson, 1966). At even higher velocities, antidunes form and migrate upstream. In the presence of antidunes, the water surface is in phase with the bed. Further increasing flow velocity results in the formation of cyclic steps, upstream migrating bedforms with hydraulic jumps forming between consecutive steps (Engelund & Hansen, 1967; Muto et al., 2012; Parker and Izumi, 2000; Simons and Richardson, 1962; Sun and Parker, 2005; Taki and Parker, 2005).

In the presence of coarse sand, ripples do not form (Simons and Richardson, 1966). At relatively small velocities, sediment is transported on a flat bed and dunes form as flow velocity increases (Engelund & Hansen, 1967). This flat bed is referred to as the *lower regime plane bed*. In the presence of coarse sand and shallow flow, an upper regime plane bed may not form and as flow velocity increases, bedforms transition from dunes to antidunes (Simons and Richardson, 1966).

The analysis of field and flume data by Naqshband, Ribberink, and Hulsher (2014) and Ohata et al. (2022) revealed that suspended bed material transport is critical for reducing dune height and transitioning to the upper plane bed. Naqshband, Ribberink, and Hulsher (2014) Figure 2 shows how threshold Froude number at the dune—upper plane bed transition decreases with increasing values of suspension number, defined as the ratio between shear velocity and settling velocity, with transition Froude numbers equal to 0.2 for values of suspension number equal to 3. The same plot shows a lack of upper plane bed data points for values of suspension number smaller than 1, corresponding to the absence of suspended bed material transport (Naqshband, Ribberink, & Hulsher, 2014).

With high resolution measurements of flow velocity and suspended bed material transport, Naqshband, Ribberink, Hurther, & Hulsher et al. (2014), Naqshband et al. (2017) explained the physics behind these observations. Bedload transport is fully trapped in each dune, thus contributing entirely to translation. Suspended bed material, on the contrary, is transported further downstream, contributing to dune deformation and thus bed flattening. Two-dimensional morphodynamic modeling based on the solution of Reynolds-averaged Navier-Stokes equations for the flow and the disequilibrium bedload transport model by Nakagawa and Tsujimoto (1980), however, revealed that the presence of suspended bed material transport is not the only reason for changes in dune geometry with flow properties (Nelson et al., 2011). The variability of particle step length with flow and bedform geometry (local bed level change) must be accounted for to properly capture bedform evolution from one bed state to another (Nelson et al., 2011).

Laboratory experiments with ~1 mm sand reported in R. R. Hernandez Moreira (2016) and R. R. Hernandez Moreira et al. (2020) showed that at flow velocities higher than those typical of the antidune regime, the bed became flat and sand was transported in a near bed layer of colliding grains with thicknesses of 10 grain diameters or more. This near bed layer is called the *sheet flow layer* (Wilson, 1987). Long bedforms with small height can form in the presence of bedload transport in sheet flow mode (R. R. Hernandez Moreira et al., 2020). These bedforms are different from those observed by Paola et al. (1989) and Bridge and Best (1988) at the dune-antidune transition. R. R. Hernandez Moreira et al. (2020) obtained bedforms with values of Froude number higher than 1.4. These bedforms did not migrate (or migrated very slowly) and emplaced structureless (massive) deposits. Bedforms described by Paola et al. (1989) and Bridge and Best (1988) were obtained with values of Froude number smaller than 1.2, migrated downstream in the absence of sheet flow and emplaced parallel laminated deposits (Best & Bridge, 1992).

Antidunes can migrate upstream and downstream (Engelund & Fredsoe, 1982; Fukuoka et al., 1982; R. R. Hernandez Moreira, 2016; R. R. Hernandez Moreira et al., 2020; Kennedy, 1961; Nunez-Gonzalez and Martin-Vide, 2010; Yokokawa et al., 2010). If upstream migration velocity is relatively small, antidunes maintain their shape. In the case of rapid upstream migration, however, antidunes grow until they become unstable, break and the bed becomes plane until a new train of upstream migrating antidunes forms (breaking antidunes) (Simons and Richardson, 1966; Yokokawa et al., 2011).

Analytical work by Engelund (1970), Fredsoe (1974), and Colombini and Stocchino (2008), empirical phase diagram by Yokokawa et al. (2011), and experiments by Spinewine et al. (2009) and Yokokawa et al. (2011) suggest that bedload transport may be important for downstream migrating antidune formation. Carling and Shvidchenko (2002) reported on downstream migrating antidunes in gravel beds with characteristic grain sizes smaller than 7 mm. Downstream migrating antidunes maintain the geometry as they travel in the direction of the flow (R. R. Hernandez Moreira, 2016) with a different scaling of their wavelength when compared to the upstream-migrating case.

3. Overview of the Experiments

Laboratory experiments were conducted in a sediment feed flume with glass walls in the Hydraulics Laboratory of the Department of Civil and Environmental Engineering at the University of South Carolina. The flume was 13 m long, 0.5 m wide and 0.9 m deep. A sediment trap was placed 9 m downstream of the flume entrance and a tailgate controlled the downstream water level. A calibrated orifice plate and a Dwyer series 490 wet-wet manometer were used to measure the flow rate from the head tank.

The flume cross-section was gradually narrowed to 0.19 cm with marine plywood in the most upstream 2 m (Figure 1). This left a 7 m long test reach, reduced the sediment volume and supply rate during experiments, as well as occurrence of three-dimensional bedforms (R. R. Hernandez Moreira et al., 2020; Jafarinik et al., 2019). A siphon rake was used to measure suspended sediment concentration profiles.

Grain size distributions of sediment supplied to the test reach or collected downstream of the sediment trap are presented in Figure 2, where legend labels indicate sand geometric mean size D_g. Two uniform quartz sands with D_g equal to 0.22 and 0.62 mm were mixed to obtain the sediment mixtures with D_g and geometric standard deviation σ_g respectively equal to 0.43 and 1.85 mm (continuous blue line) and 0.34 and 1.95 mm (continuous red line). Purple sand that can be seen in pictures and videos corresponds to the 0.62 mm sand (black line in Figure 2).

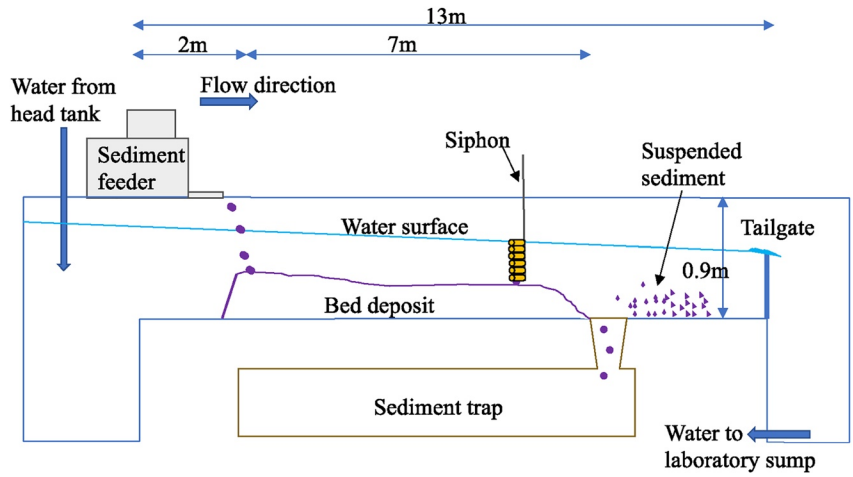

Figure 1. Schematic representation of the laboratory flume. Drawing not to scale.

Sediment collected downstream of the sediment trap is representative of sediment transported in suspension (dash lines in Figure 2).

Experiments are summarized in Table 1 in terms of D_g and D_{90} of the sediment fed into the flume, flow rate Q_w, and mass feed rate G_s, with D_{90} denoting the diameter such that 90% of the sediment is finer. Part of the sediment fed into the flume was transported as bedload transport (typically coarse fractions) and the rest was transported in suspension. Thus, at equilibrium G_s represented the total (bedload plus suspended load) mass transport rate of bed material.

Experiments are named with a number and name initials of the lead experimentalist; for example, 1-SS denotes the first experiment ran by Sydney Sanders and 9-SJ denotes the ninth experiment ran by Sadegh Jafarinik. Experiments 1-SJ–4 SJ were performed to investigate the role of water depth (flow rate) on upper regime bedforms. Experiments 5-SJ to 9-SJ and 1-SS to 7-SS were designed to study the role of sand transport mode in upper regime equilibrium configurations. The experimental database of Table 1 was integrated with experiments by R. R. Hernandez Moreira (2016) and R. R. Hernandez Moreira et al. (2020) to study the role of sediment caliber in bedform type and geometry.

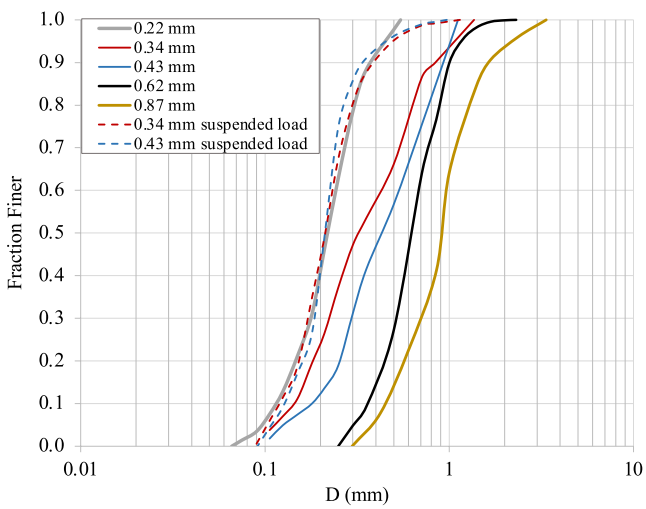

Figure 2. Grain size distributions of the sediment used in the experiments. Legend labels correspond to the sand geometric mean diameter D_g. Dashed lines are grain size distributions representative of suspended sand load in the SS experiments.

4. Experimental Procedure

Experiments started from a condition of disequilibrium (net-depositional or net-erosional) and continued until flow and sediment transport reached equilibrium. At equilibrium, suspended sediment concentration was measured, and the experiment was terminated. Experiments 1-SJ, 5-SJ, and 8-SJ started with a nearly empty flume. Few bags of sand were emptied to cover the flume bottom and favor sediment deposition in the test reach (Johnson et al., 2014). Experiment 1-SS started with a 10 cm thick layer of 0.43 mm sand. Initial conditions of experiments 2-SJ to 4-SJ, 6-SJ, 7-SJ, 2-SS, 3-SS, and 5-SS to 6B-SS were equilibrium deposits from previous experiments. For example, the initial bed of experiment 3-SJ was the equilibrium bed at the end of experiment 2-SJ. After experiment 3-SS, an approximately 3 cm thick layer of sand with D_g equal to 0.34 mm was sprinkled over the existing deposit to perform experiments with a finer sediment grain size. This process was repeated before experiment 7-SS by sprinkling instead coarse sediment with D_g equal to 0.62 mm. The duration of each experiment varied between 45 min to 2 hr depending on the time required to reach equilibrium.

Bed evolution from one equilibrium state to the other was characterized by observation and measurements of bed and water surface elevations, as done in previous experimental studies on open-channel flow bedforms by

Table 1
Summary of Experimental Conditions

Run name	D_g (mm)	D_{90} (mm)	Q_w (l/s)	G_s (kg/min)
1-SJ	0.87	1.68	15	1.5
2-SJ	0.87	1.68	15	6
3-SJ	0.87	1.68	15	16
4-SJ	0.87	1.68	8	6
5-SJ	0.62	1.10	15	1
6-SJ	0.62	1.10	15	2.2
7-SJ	0.62	1.10	15	6.9
8-SJ	0.22	0.38	15	0.6
9-SJ	0.22	0.38	8	0.6
10-SJ	0.22	0.38	8	2.2
1-SS	0.43	0.93	30	10
2-SS	0.43	0.93	20	10
3-SS	0.43	0.93	10	10
4-SS	0.34	0.84	10	10
5-SS	0.34	0.84	10	15
6A-SS	0.34	0.84	10	20
6B-SS	0.34	0.84	5	20
7-SS	0.62	1.10	10	10

Note. Experiments were run in two different experimental sets and are denoted by the lead experimentalist's initials (i.e., SS and SJ) along with each unique run number where Experiment 1 ran by Sydney Sanders is denotated as 1-SS and Experiment 3 ran by Sadegh Jafarinik is denoted 3-SJ. D_g denotes the geometric mean diameter of the sediment used in each experiment, Q_w is the flow discharge and G_s the total (bedload plus suspended load) mass sediment feed rate.

Kennedy (1961), Simons and Richardson (1962, 1966), Guy et al. (1966), Task Force on Bed Forms in Alluvial Channels (1966), Fukuoka et al. (1982), and R. R. Hernandez Moreira et al. (2020) among many others. Bedform height, length, and migration rate were measured using rulers attached to the flume and from the analysis of video recordings.

If the bed and water surface were in opposition to phase, bedforms were classified as washed-out dunes WD because of the relatively high (but still subcritical) Froude number. If the bed and water surface were in phase, migrating bedforms were classified as antidunes and non-migrating bedforms were considered standing waves (SW). Depending on the direction of migration, antidunes were classified as upstream UA or downstream migrating DA. Plane bed configurations were classified on the basis of bedload transport mode, that is, upper plane bed with a few grain diameters thick bedload layer UP or upper plane bed with bedload transport in sheet flow mode PS.

4.1. Measurements of Bed and Water Surface Profiles and Flow Resistance

Vertical rulers on the glass wall and horizontal rulers on top of the flume indicated elevation above the flume bottom and distance from the flume entrance respectively. Bed and water surface elevations were measured with ruler readings at streamwise intervals of 10 cm in the SJ experiments and 20 cm in the SS experiments. The first measurement was recorded at 2.2 m from the flume entrance in SJ experiments and at 3.5 m in SS experiments. The last measurement was taken approximately at 8.85 m from the flume entrance.

During each experiment, measured elevations were reported in a spreadsheet, plotted, bed slope and water surface slope were estimated with best fit lines. When bed and water surface slopes did not significantly change in time, the flow and the sediment transport were deemed to be at equilibrium (R. R. Hernandez Moreira et al., 2020; Viparelli et al., 2015). Equilibrium water depth and bed slopes were respectively determined as the average difference between measured water surface and bed elevation and the slope of the best fit line of the last measured longitudinal profile.

Experiments were performed with water depths varying between 0.04 and 0.13 m. The width to depth ratio was thus smaller than 5 and the cross section was considered narrow. In a narrow cross section, different roughness between sediment covered bed and smooth side walls must be accounted to estimate the shear stress acting on the bed (Vanoni and Brooks, 1957). Here, we followed the procedure to remove sidewall effects from measured data introduced by Vanoni and Brooks (1957) as formulated by Chiew and Parker (1994).

In the presence of bedforms, flow resistance is the result of friction introduced by the granular bed (skin friction) and flow separation at bedform crests (form drag). Stresses that act tangentially to the bed, known as skin friction, are critical to sediment entrainment and bedload transport. When no bedforms are present, the drag on the bed is associated only with skin friction (Einstein & Barbarossa, 1952; Parker, 2004). For the partition of flow resistance between skin friction and form drag, an ideal flat bed configuration was considered. This ideal flow had the same grain roughness, energy slope, and mean flow velocity as those in the presence of bedforms (Parker, 2004). For further details, we refer to the Supporting Information S1 file Data Set S1 that was used to analyze the data.

4.2. Measurements of Suspended Sediment Concentration

The volumetric suspended sediment concentration, c, was measured with a rack of six plastic siphons located approximately 2 cm apart. No attempt was made to sample isokinetically. Similar devices and sample strategies were used in previous experimental studies such as, for example, those by Parker et al. (1987), Garcia (1990),

Table 2
Summary of Experimental Results, Where S = Bed Slope, H = Flow Depth, Δ = Bedform Height, λ = Bedform Wavelength, v = Migration Rate, Negative Values Indicate Upstream Migrating Bedforms, U = Mean Flow Velocity, Fr_o = Sidewall Corrected Froude Number Associated With Skin Friction, u and u_o^* Respectively Denote the Sidewall Corrected Values of Shear Velocity and Shear Velocity due to Skin Friction*

Run	S (–)	H (cm)	Δ (cm)	λ (cm)	v (cm/min)	$\boldsymbol{U}$ (m/s)	Fr_o (–)	u^* (cm/s)	u_o^* (cm/s)	Bed configuration
1-SJ	0.0057	8.70	1.8	33	35	0.91	1.05	5.65	5.65	WD
2-SJ	0.0110	6.16	1.5	30	60	1.28	1.76	6.74	6.74	DA
3-SJ	0.0211	5.32	0.5	45	18	1.48	2.15	9.15	9.15	PS
4-SJ	0.0178	3.97	–	65	–	1.06	1.75	7.59	7.59	UP
5-SJ	0.0049	10.27	2.8	38	30	0.77	0.84	5.86	5.39	WD
6-SJ	0.0074	7.91	3.2	25	29	1.00	1.21	6.26	6.26	DA
7-SJ	0.0135	4.87	–	35	–	1.62	2.55	6.22	6.22	UP
8-SJ	0.0024	10.17	0.8	10	17	0.78	0.89	3.25	3.25	WD
9-SJ	0.0029	8.42	1.0	10	18	0.50	0.63	4.24	3.20	WD
10-SJ	0.0049	6.36	1.8	28	17	0.66	0.92	4.81	4.22	UA/SW
1-SS	0.0072	13.14	–	0	–	1.20	1.16	7.27	7.27	UP
2-SS	0.0080	12.91	1.0	65	–	0.82	0.87	8.88	5.87	SW
3-SS	0.0150	3.96	2.0	50	−35	1.33	2.25	6.52	6.52	UA-breaking
4-SS	0.0140	4.09	3.0	50	−130	1.29	2.14	6.39	6.39	UA
5-SS	0.0130	4.98	4.5	80	−150	1.06	1.58	7.05	7.05	UA
6A-SS	0.0150	5.52	5.5	90	–	0.95	1.41	8.23	7.06	UA-breaking
6B-SS	0.0180	3.89	3.0	100	–	0.68	1.24	7.92	5.66	UA-breaking
7-SS	0.0110	5.92	1.0	55	−18	0.89	1.24	7.18	6.67	UA

Note. Bed configuration is reported using the following abbreviations: WD for washed-out dunes, UP for upper plane bed with a few grain diameters thick bedload layer, SW for standing waves, UA for upstream migrating antidunes, DA for downstream migrating antidunes, and PS for upper plane bed with bedload transport in sheet flow "mode. "–" indicates that bedform height or migration rate were not measured.

Mohrig et al. (1998), Toniolo et al. (2006), and Sequeiros et al. (2009, 2010). Samples were collected in 1,500 cm^3 containers, the suspension was filtered, sediment was dried, weighted and volumetric concentration was computed. To convert sediment weight into volumes, a density equal to 2.65 gr/cm^3 was used.

Measurements of suspended sediment concentration were performed in experimental runs 1-SS to 6B-SS, 5-SJ to 7SJ, 9-SJ, and 10-SJ. In SJ experiments, the rack was placed at 8.2 m from the flume entrance and the distance between the siphon closest to the deposit and the deposit was kept equal to few percent of the flow depth. In the SS experiments, the rack was placed close to the downstream end of the deposit. The distance between the siphon closest to the deposit and the deposit varied from one experiment to another because the rack was anchored to the flume sidewalls.

5. Results

Experimental results are summarized in Table 2 in terms of equilibrium bed slope S, flow depth H, bedform height Δ, bedform length λ, migration rate v, depth-averaged flow velocity U, Froude number associated with skin friction Fr_o, sidewall corrected shear velocity u^*, shear velocity associated with skin friction u_o^* and bed configuration. As expected, the equilibrium slope increases with the sediment supply rate and consequently, equilibrium flows get shallower and faster (see, e.g., experiments 1-SJ, 2-SJ, and 3-SJ). In response to an increase in flow rate, on the contrary, the equilibrium slope decreases and equilibrium flow becomes deeper than in case of comparatively smaller discharges (see, e.g., experiments 1-SS, 2-SS, and 3-SS).

A close look at Table 2, however, reveals that such straightforward arguments for equilibrium are not always applicable because the presence of bedforms clearly complicates the problem. For example, in experiments 4-SS,

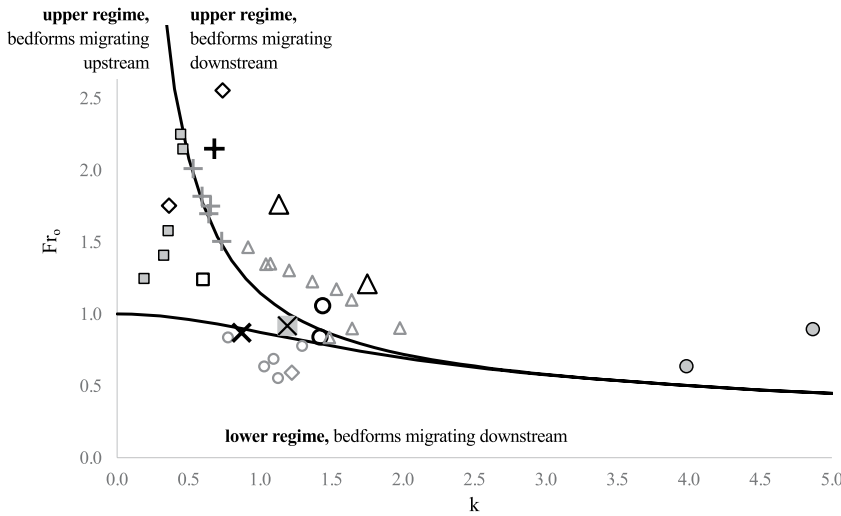

Figure 3. The Engelund phase diagram after Parker (2004) with the experiments of Table 2 (black marker line) of Hernandez Moreira (2016) and Hernandez Moreira et al. (2020) (gray marker line). Empty symbols indicate experiments with coarse sand ($D_g > 0.5$ mm) and symbols with gray fill are experiments with fine sand ($D_g \leq 0.5$ mm). Circles represent washed out dunes, diamonds denote upper plane bed conditions, triangles are downstream migrating antidunes and squares indicate upstream migrating antidunes. "x" represents standing waves (SW) (experiment 2-SS), "x" with a gray background indicates conditions at the transition between SW and upstream migrating antidunes (experiment SJ-10) and "+" indicates upper plane bed with bedload transport in sheet flow mode.

5-SS, and 6-SSA, sediment type and discharge did not change, and the sediment feed rate increased from 10 to 20 kg/min. This notwithstanding, the bed slope did not change significantly, and the water depth increased in response to a change in bedform geometry.

5.1. Bedform Classification

The Engelund phase diagram after Parker (2004) (see also Figures 2–37 in Garcia, 2008 and Figure 2 in Muto et al., 2012) is utilized to compare our bedform classification based on observations of bed and water surface, with a well-established classification criterion (Figure 3). Bedforms are classified based on Fr_o and non-dimensional wavenumber k defined as $2\pi H_o/\lambda$, where H_o is the flow depth associated with skin friction (Colombini & Stocchino, 2008). Black lines in Figure 3 identify three regions of the (k, Fr_o) plane corresponding to the lower and upper regimes with bedform migrating upstream or downstream. Most data pertaining to experiments with fine sand are found in the region of upstream migrating bedforms. Data of upper regime experiments with coarse sand are in the region of downstream migrating bedforms or close to the boundary between upstream and downstream migrating waves (Figure 3).

Upstream migrating antidunes were further classified as stable or breaking. Figures 4a and 4b and Movie S1 show upstream migrating antidunes with stable geometry in experiments 5-SS and 7-SS. In experiment 4-SS, bed and water surface deformation was larger than in experiments 5-SS and 7-SS. Water surface amplitude periodically became so large that surface wave broke, and the bed locally flattened (Figure 4c, and Movie S2). In experiments 3-SS, 6A-SS, and 6B-SS, the deformation of the alluvial bed became so strong that waves formed, grew, broke and the bed became flat until a new train of upstream migrating antidunes formed. These bedforms are called breaking antidunes, following Simons and Richardson (1966), and are shown in Figure 4d (experiment 3-SS), Figures 4e and 4f (experiment 6B-SS), and in Movie S3 and S4.

Measurements of suspended sediment concentration are presented in Figure 5 in plots of volumetric suspended sediment concentration c against non-dimensional elevation above the channel bed z/H. In experiments with upstream migrating antidunes, the volumetric suspended sediment concentration was about one order of magnitude higher than in experiments with other bed configurations. At high flow velocities typical of an antidune regime, our experiments show that sand with grain size smaller than 0.3 mm was preferentially transported in suspension and sand with grain size coarser than 0.3 mm was preferentially transported as bedload, as shown by

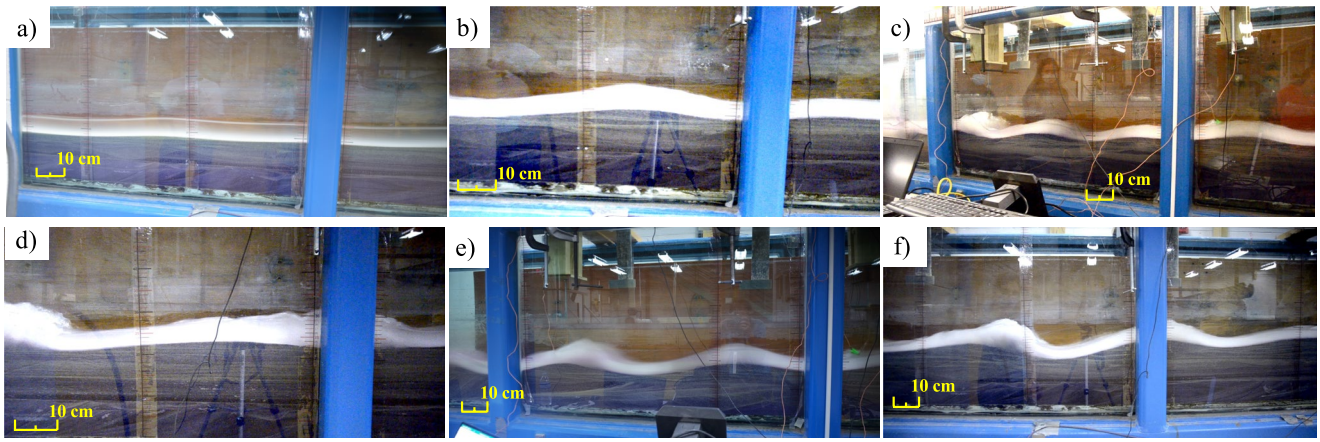

Figure 4. Breaking and non-breaking upstream migrating antdunes in experiments (a) 7-SS, (b) 5-SS, (c) 4-SS, (d) 3-SS, (e) 6B-SS, and (f) 6B-SS.

sediment samples in Figure 2 and by the absence of purple sand (D_g = 0.62 mm) in suspended sediment samples. It is important to note here that fine sand did not behave as wash load, as shown by the significant presence of white sediment in the deposits of Figure 3 and of the Supporting Videos.

5.2. Role of Sediment Size and Supply on Bedform Geometry and Progression

Pictures taken during experiments 4-SS, 5-SS, and 6A-SS with fine sand (D_g = 0.34 mm) are given in Figure 6. When the total sediment transport rate increased from 10 to 15 to 20 kg/min and the flow rate was kept equal to 10 l/s, the antidune length increased from 50 to 80 cm and height increased from 3 to 5.5 cm, as upstream-migrating antidunes (4-SS and 5-SS) evolved into breaking antidunes (6A-SS). As the sediment load increased with a constant flow rate, Table 2 shows an increase in overall flow resistance, as suggested by the increasing total shear velocity along with changes in flow velocity (decrease), flow depth (increase), and Froude number (decrease).

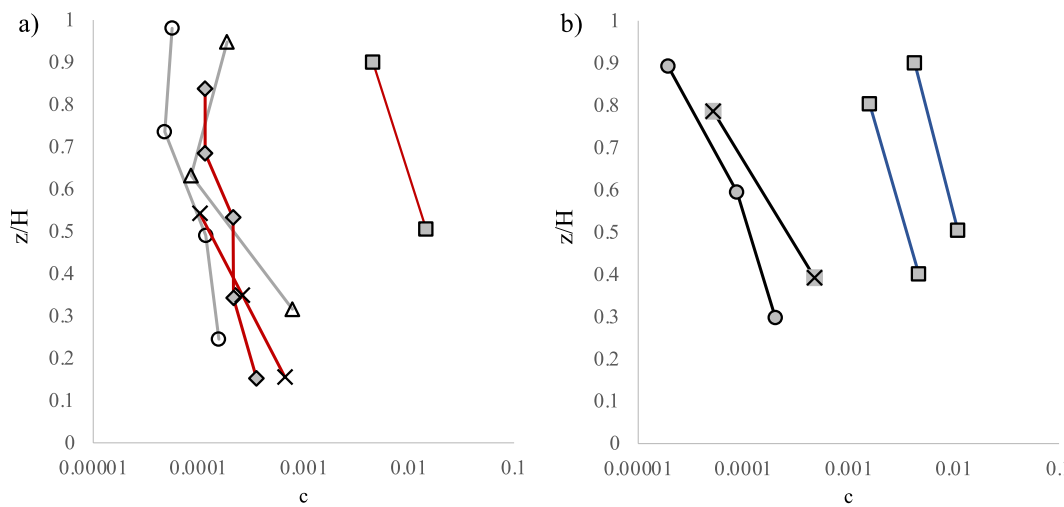

Figure 5. Profiles of suspended sediment concentration measured during experiments 1-SS–5-SS, 5-SJ, 6-SJ, 9-SJ, and 10-SJ. z denotes an upward oriented vertical coordinate with origin on the channel bed, H the water depth and c the volumetric suspended sediment concentration Line color indicates sand geometric mean size and symbols indicate the bed configuration. Gray, red, blue and black lines represent experiments with sand D_g equal to 0.62, 0.43, 0.34, and 0.22 mm, respectively. As shown in Figure 4, circles, triangles, diamonds, "x" and squares respectively denote bed configurations of washed out dunes, downstream migrating antidunes, plane beds, standing waves (SW) and upstream migrating antidunes. Empty symbols indicate experiments with coarse sand (D_g > 0.5 mm) and symbols with gray fill are experiments with fine sand ($D_g \leq$ 0.5 mm). The "x" symbol with a gray background indicates the transition between SW and upstream migrating antidunes of Experiment 10-SJ.

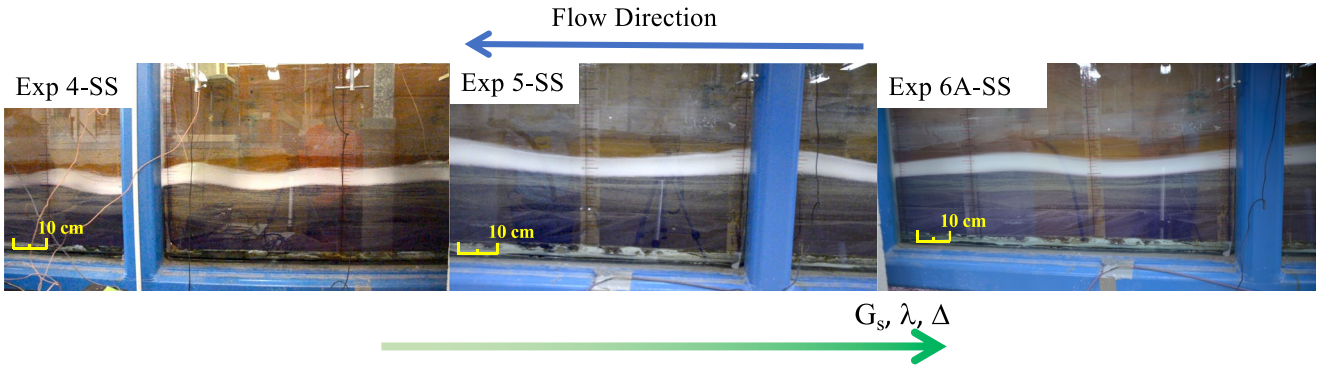

Figure 6. Pictures of experiments with fine sand (D_g = 0.34 mm). As the mass feed rate G_s increases, bedform wavelength λ and height Δ increase.

The equilibrium slope increased from upstream migrating antidunes (4-SS and 5-SS) to breaking antidunes (6A-SS).

In experiments with coarse sand, we also observed bedform length increasing with increasing sediment transport rate. Runs 2-SJ and 3-SJ were performed using sand with D_g equal to 0.87 mm. In these runs, the bedform length increased from 30 to 45 cm as the transport rate increased from 6 kg/min to 16 kg/min (same flow rate). In runs 6-SJ and 7-SJ, sand had D_g equal to 0.62 mm and as the transport rate increased from 2.2 to 6.9 kg/min (same flow rate), the bedform length also increased from 25 to 35 cm, as shown in Figure 7.

In contrast to fine sand experiments, however, bedform height decreased with increasing sediment supply for all coarse sand experiments. Increasing sediment supply rate resulted in bedform progression from washed-out dunes to downstream migrating antidunes and plane bed with bedload transport in sheet flow mode in experiments 1-SJ to 3-SJ (lower to upper regime transition and downstream migrating to sheet flow transition). In experiments 5-SJ to 7-SJ, equilibrium bed configuration varied from WD, to downstream-migrating antidunes, to upper plane beds with a few grain diameter thick bedload layer (lower to upper regime transition). When sediment transport rate increased to 10 kg/min and flow discharge decreased from 15 to 10 l/s, on the other hand, plane bed of experiment 7-SJ evolved into upstream migrating antidunes of experiment 7-SS.

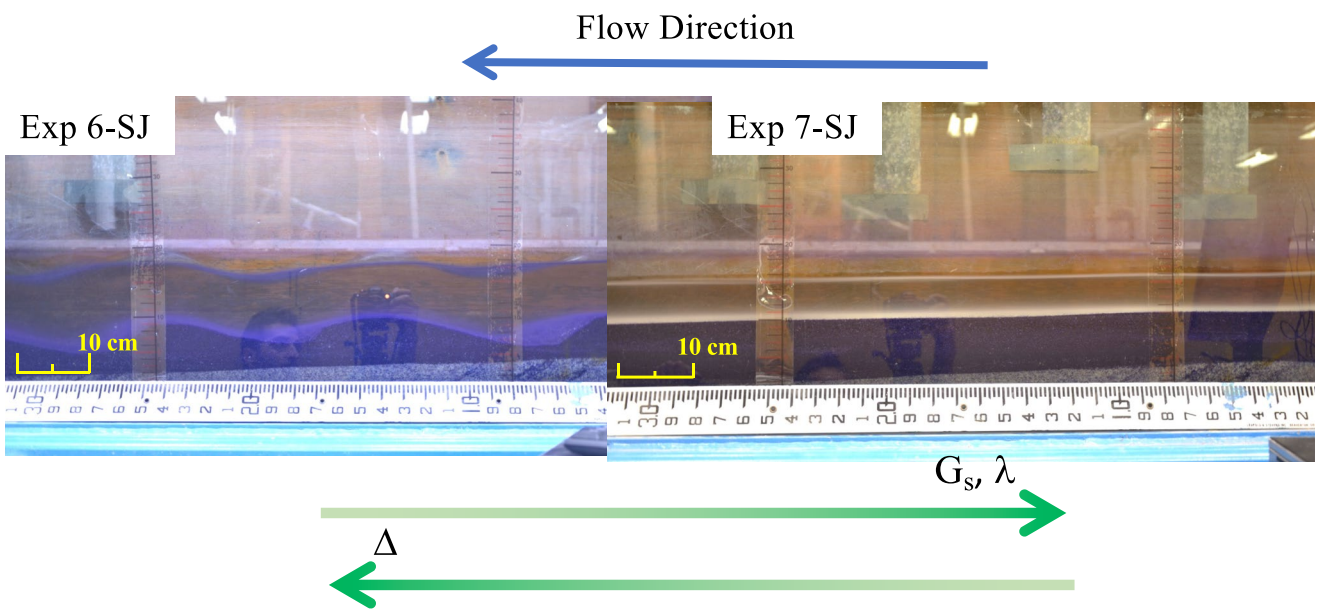

Figure 7. Pictures of experiments with coarse sand (D_g = 0.62 mm). As the mass feed rate G_s increases, bedform wavelength λ increase and bedform height Δ decreases.

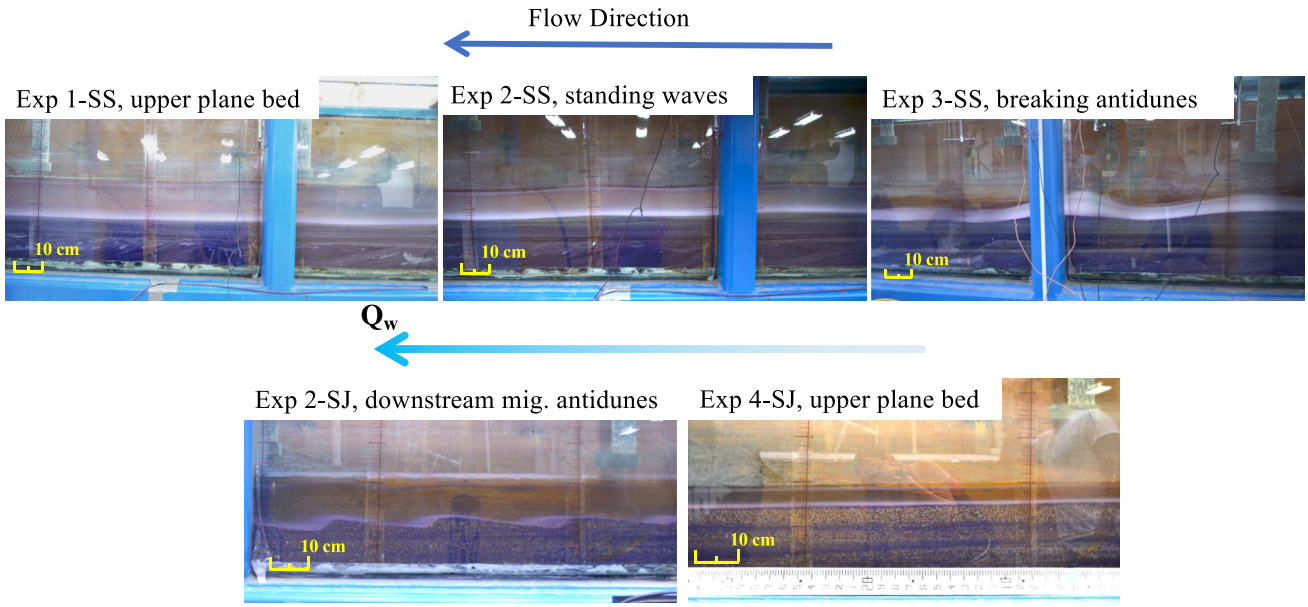

Figure 8. Pictures showing a change in equilibrium bed configuration with the water discharge Q_w.

5.3. Role of Flow Discharge on Equilibrium Bedforms

In experiments 1-SS, 2-SS, and 3-SS, flow discharge decreased from 30 to 20 to 10 l/s, sediment transport rate was kept at 10 kg/min, and sand D_g was 0.43 mm. This reduction in flow discharge caused an increase in equilibrium bedform height and the following bedform progression: upper plane bed with a few grain diameters thick bedload layer in experiment 1-SS, SW in experiment 2-SS, and upstream migrating antidunes in experiment 3-SS (Figure 8). In experiments 2-SJ and 4-SJ, flow discharge decreased from 15 to 8 l/s and bed configuration changed from downstream migrating antidunes to upper plane bed with a few grain diameters thick bedload layer (Figure 8). Furthermore, a change in flow discharge was not always associated with a change in bedform type: for example, in experiments 6A-SS and 6B-SS, as Q_w decreased from 10 to 5 l/s, observed configurations of breaking antidune height decreased from 5.5 to 3 cm and length increased from 90 to 100 cm.

A change in antidune migration direction induced by a change in water discharge and sediment size was observed in experiments 6-SJ and 10-SJ. Water discharge decreased from 15 l/s (6-SJ) to 8 l/s (10-SJ) and D_g decreased from 0.62 mm (6-SJ) to 0.22 mm (10-SJ). Antidunes migrated downstream in run 6-SJ, whereas bedforms in run 10-SJ were close to the standing wave-antidune transition and slowly migrated upstream. Equilibrium slope, water depth, flow velocity, bed shear velocity, and Froude number decreased when comparing 10-SJ to 6-SJ (i.e., as both discharge and sediment caliber decreased), but a first order estimate of the overall flow resistance showed an unexpected increase from 10-SJ to 6-SJ. The effect of sediment size on upstream migrating antidunes was also observed by comparing experiments 3-SS, 4-SS, and 7-SS with $Q_w = 10$ l/s and $G_s = 10$ kg/min. Bedform length did not change with sediment size (~50 cm), but antidune height was the highest and migration rate was fastest with the finest sediment size (experiment 4-SS).

5.4. Comparison With Previous Experiments Performed in the Same Flume

Results of the experiments in Tables 1 and 2 are summarized as follows: An increase in sediment transport rate caused an increase in upstream migrating antidune height and length (Figure 6). In experiments with coarse sand, increasing sediment transport rate resulted in longer and smaller equilibrium bedforms with a transition from WD to downstream migrating antidunes to a plane bed with either a few grain-diameter-thick bedload layer or sheet flow (Figure 7).

Reducing flow discharge from 30 to 10 l/s in experiments with fine sand caused bedform progression from the upper plane bed to SW to upstream migrating antidunes. Further reducing flow discharge to 5 l/s resulted in smaller antidune height in experiments 6B-SS than in 6A-SS. Decreasing water discharge from 15 to 8 l/s in

Table 3
Comparison Between Bedform Height Δ, Wavelength λ and Bed Configuration in Experiments Performed With Coarse Sand With D_g = 0.87 mm (SJ) and D_g = 1.11 mm (RHM)

Run name	Q_w (l/s)	G_s (kg/min)	Δ (cm)	λ (cm)	Bed configuration
1-SJ	15	1.5	1.8	33	WD
RHM	20	1.5	3.8	78	WD
RHM	30	1.5	4.0	77	WD
2-SJ	15	6	1.5	30	DA
RHM	30	6	5.0	42	DA
3-SJ	15	16	0.5	45	PS
RHM	20	16	1.0	70	PS
RHM	30	16	4.0	80	PS

Note. Q_w denotes the flow discharge and G_s the mass feed rate. Bed configuration is reported using the following abbreviations: WD as washed-out dunes, DA as downstream migrating antidunes, and PS as upper plane bed with bedload transport in sheet flow mode.

coarse sand experiments resulted in a transition from downstream migrating antidunes to the plane bed.

R. R. Hernandez Moreira (2016) and R. R. Hernandez Moreira et al. (2020) noticed a similar behavior in upper regime experiments with coarse sand. As the sediment transport rate increased, downstream migrating antidunes became longer. At transport rates higher than 10 kg/min, variations in bedform geometry were associated with the development of the sheet flow layer (R. R. Hernandez Moreira, 2016; R. R. Hernandez Moreira et al., 2020).

Experiments 1-SJ, 2-SJ, and 3-SJ are compared with experiments by R. R. Hernandez Moreira (2016) with the same sediment transport rate and similar sediment size. Changing the flow discharge from 30 to 15 l/s did not modify the bed configuration. However, bedform height and length in experiments with Q_w equal to 15 l/s were smaller than in the experiments with Q_w equal to 20 and 30 l/s, as shown in Table 3, where Hernandez Moreira experiments are denoted as RHM. Reducing flow discharge from 30 to 20 l/s did not impact washed out dune height but caused a height reduction of long bedforms in experiments with bedload transport in sheet flow mode (PS).

5.5. Non-Dimensional Summary of Experiments

Results of experiments presented above, in R. R. Hernandez Moreira (2016) and R. R. Hernandez Moreira et al. (2020) are summarized in Figure 9 in terms of (a) ratio Q_s/Q_w between volumetric total (bedload plus suspended load) bed material (sand) load and flow discharge, (b) sediment size in terms of fine sand ($D_g \leq 0.5$ mm or particles Reynolds number $Re_p \leq 45$) or coarse sand ($D_g > 0.5$ mm, $Re_p > 45$), (c) bed configuration, (d) non-dimensional bedform length λ/H and λ/D_g respectively in panels a and b, and height Δ/H in panel c, and (e) ratio between shear velocity u^* and settling velocity of sand geometric mean size v_s in panel d, with $u^*/v_s = 0.8$ indicating the threshold value for significant suspension (Bagnold, 1966). Particle Reynolds number is a non-dimensional grain size defined as $Re_p = \sqrt{RgD}D/\nu$ with R being the sediment submerged specific gravity equal to 1.65, g the acceleration of gravity and ν the kinematic viscosity of water. Quantitative details on the agreement between the proposed bedform classification, the criterion for significant suspension and the data are in Text S1 and S2 in Supporting Information S1.

5.5.1. Bedform Progression

Equilibrium bed configurations in Figure 9 are WD, upper plane bed with a few grain diameters thick bedload layer (UP), downstream migrating antidunes (DA), SW, upper regime plane bed with bedload transport in sheet flow mode (PS) and upstream migrating antidunes (UA). In agreement with what observed in fine sand (Engelund & Hansen, 1967), as Q_s/Q_w increases equilibrium configuration transitions from lower to upper regime (Simons and Richardson, 1962). Our data suggest that this transition occurs for Q_s/Q_w between 0.0003 and 0.0007.

A second transition characterizes the upper regime. For Q_s/Q_w smaller than 0.0015, antidunes migrated downstream. When Q_s/Q_w was larger than 0.0032, two equilibrium bed configurations were observed. Upstream migrating antidunes formed in experiments with fine sand. A plane bed with bedload transport in sheet flow mode characterized equilibrium in experiments with coarse sand. This type of plane bed was also recognized by Ohata et al. (2022), who did not include it in their re-analysis of plane bed configurations for the paucity of experimental data. An upper plane bed with a few grain diameters thick bedload layer occurred in 3 out of 4 cases in the transition regions. Standing waves occurred for values of Q_s/Q_w between 0.0015 and 0.0032. Breaking antidunes occurred for the highest values of Q_s/Q_w suggesting that at such high values of Q_s/Q_w antidunes become unstable and may transition toward a different bed configuration.

5.5.2. Bedform Geometry

As Q_s/Q_w increased and equilibrium bed configuration transitioned from washed out dune to upper regime, λ/H remained relatively unchanged with bedform length equal, on average, to 3–4 times the water depth (Figure 9a), a value that is of the same order of magnitude as the average value reported in Naqshband, Ribberink, and Hulsher (2014). On the contrary, non-dimensional length λ/D decreased, indicating that bedforms shortened

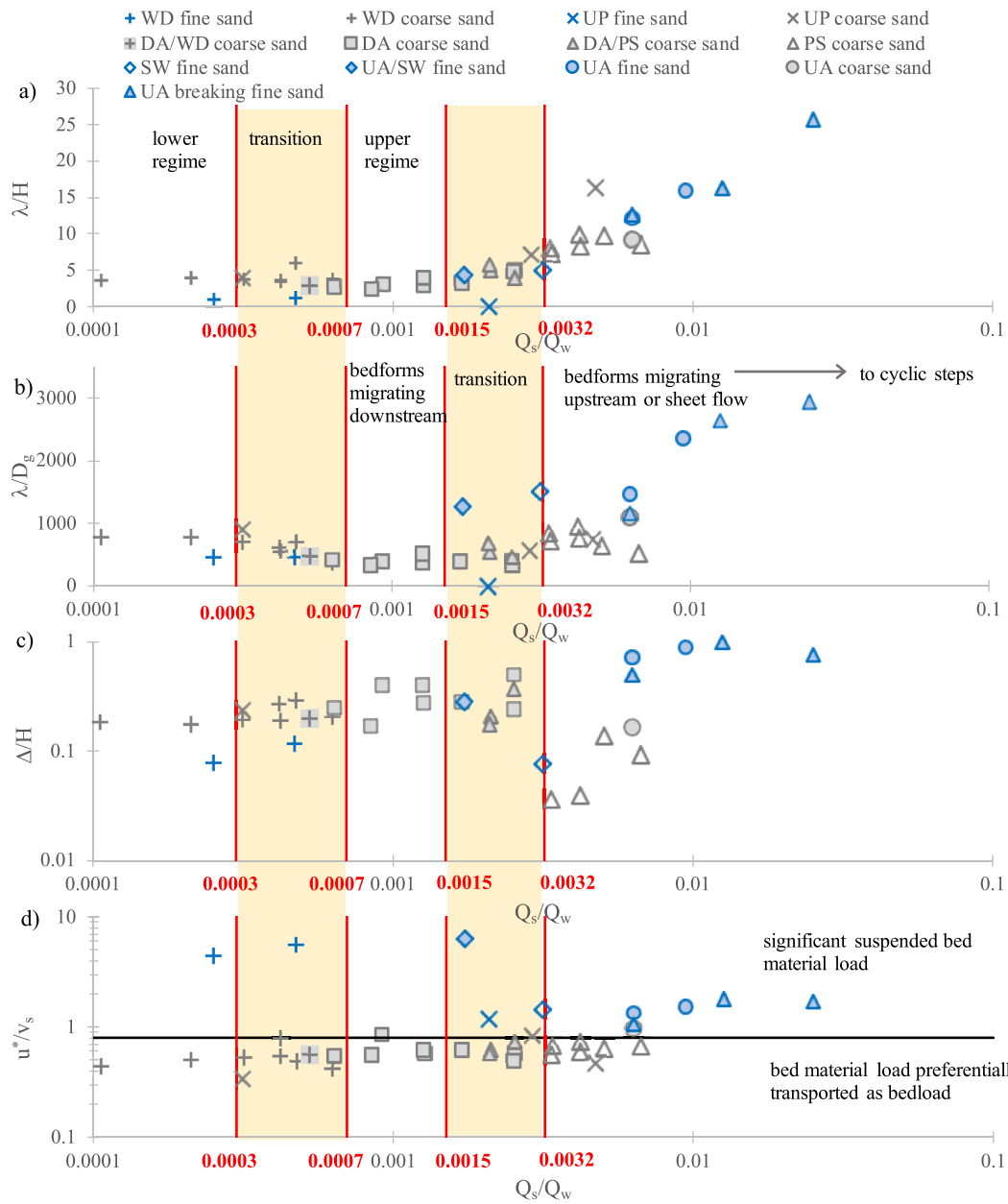

Figure 9. Non-dimensional summary of the experiments presented in this paper, in Hernandez Moreira (2016) and Hernandez Moreira et al. (2020). Q_s/Q_w is the ratio between volumetric bed material load and flow discharge, H denotes water depth, λ bedform wavelength, D characteristic sediment size, Δ bedform height, u^* shear velocity, v_s settling velocity of sand with geometric mean size D_g. Here, fine sand has $D_g \leq 0.5$ mm (blue symbols), and coarse sand has $D_g > 0.5$ mm (gray symbols). Line symbols indicate lower regime bedforms (washed out dunes WD) and upper regime plane bed with a few grain-diameter-thick bedload layer UP. Symbol shapes indicate upper regime bedforms, with open shapes denoting stationary (or slowly moving) bedforms such as standing waves (SW) and upper plane beds with bedload transport in sheet flow mode PS. Filled shapes indicate migrating bedforms such as downstream migrating antidunes DA and upstream migrating antidunes UA, bed configurations at the downstream migrating antidune—standing wave transition DA/SW, at the upstream migrating antidune—standing wave transition and UA/SW and at the transition between downstream migrating antidunes and upper regime plane bed with bedload transport in sheet flow mode DA/PS.

across the lower regime—upper regime transition (Figure 9b). Equilibrium bedform length increased across the transition from downstream migrating antidunes to upstream migrating antidunes and sheet flow. This suggests that in fine sand at values of Q_s/Q_w higher than those considered here, upstream migrating bedforms may be very

long, corresponding to cyclic steps, also known as chutes and pools (Figure 9, panels a and b), or even transitioning to a more generalized plane bed as finer material can be readily entrained into suspension. As suggested by some experimental evidence, an increase in sediment concentration can dramatically change bedform mechanics (e.g., Wright and Parker, 2004a, 2004b).

Non-dimensional bedform height Δ/H increased with Q_s/Q_w from washed out dune to the limit between downstream and upstream migrating bedforms. In particular, Δ was approximately equal to 20% of the flow depth in washed out dune experiments and increased up to 50% of H in the experiments with downstream migrating antidunes, ranges that are comparable with those reported by Naqshband, Ribberink, and Hulsher (2014). For values of Q_s/Q_w greater than 0.0032, Δ/H increased in experiments with fine sand and decreased in the experiments with coarse sand (see also Figures 6 and 7).

5.5.3. Mode of Sand Transport

The ratio u^*/v_s on the vertical axis of Figure 9d is used to distinguish experiments in which sand was not suspended $u^*/v_s < 0.8$, from those with significant suspended sand load, $u^*/v_s > 0.8$ (Bagnold, 1966), with v_s being the settling velocity of the geometric mean size of the sediment fed into the flume. This criterion correctly predicts the suspended sand load in 13 experiments. It does not capture the presence of a suspended load in experiment 5-SJ only. Further, in agreement with experimental observations, it correctly predicts suspended sand load in all experiments with upstream migrating antidunes and does not predict suspension in 17 of the 18 experiments with downstream migrating antidunes and bedload transport in sheet flow mode (Figure 5, R. R. Hernandez Moreira, 2016; R. R. Hernandez Moreira et al., 2020). In summary, Figure 9d suggests that suspended sand load may be important for the development of equilibrium upstream migrating bedforms, in agreement with Engelund (1970), Fredsoe (1974), Colombini and Stocchino (2008) and with recent analytical work by Ohata et al. (2021).

6. Discussion

6.1. Comparison With Other Datasets

To determine if bedform progression of Figure 9 can be generalized to other open channel flow and submarine experiments, we plotted data by Kennedy (1961), Guy et al. (1966), and Fukuoka et al. (1982) pertaining to subaerial (open-channel) antidunes, SW, upper plane bed and cyclic steps. We also considered data by Fedele et al. (2016) pertaining to subaqueous (saline and turbidity currents). Figure 10 includes non-dimensional plots analogous to those in Figure 9 but for the above-mentioned data sets. In the submarine case, only a few experiments were available from all those reported in Fedele et al. (2016) due to the combined availability of suspended sediment concentration and videos, from which bedform migration speeds were taken to reliably estimate sediment transport rates. In addition, videos and a few reliable velocity profiles available were used to estimate the thickness of the denser layer of the flow, which was used as the relevant flow-related vertical length scale H. The submarine cases include both downstream and upstream migrating antidunes.

Transition zones between lower and upper regime ($0.0003 < Q_s/Q_w < 0.0007$) and between upper regime bedforms migrating downstream and upper regime bedforms migrating upstream or the presence of a sheet flow layer ($0.0015 < Q_s/Q_w < 0.0032$) well represent the equilibrium bed configurations of Figure 10 for all these data sets, including the subaqueous cases. Points representing SW for the subaerial cases are in the transition zone with $0.0015 < Q_s/Q_w < 0.0032$. Many upstream migrating bedforms, including equilibrium cyclic steps, are correctly predicted for $Q_s/Q_w > 0.0032$. For the submarine cases, downstream-migrating antidunes are correctly predicted within the proposed range of $Q_s/Q_w < 0.0032$ and long upstream migrating submarine sediment waves occur for values of Q_s/Q_w larger than those characterizing cyclic steps in open channel flow experiments (see Normark et al., 2002 and Kostic, 2014 for possible field analogues).

The proposed classification criterion correctly predicts the upper regime ($Q_s/Q_w > 0.0003$) for all open-channel (subaerial) 109 points representing plane bed with Fr > 0.65, SW, antidunes, chutes and pools (cyclic steps) by Guy et al. (1966). It further correctly classified 38 of the 43 experiments by Kennedy (1961) and 60 of the 64 experiments by Fukuoka et al. (1982). Five WD in experiments by Kennedy (1961) and four dunes in experiments by Fukuoka et al. (1982) were misclassified as upper regime bedforms.

The distinction between downstream and upstream migrating bedforms ($Q_s/Q_w > 0.0015$) also agrees with other experimental observations, including the submarine bedform cases. All subaerial cyclic steps are well classified

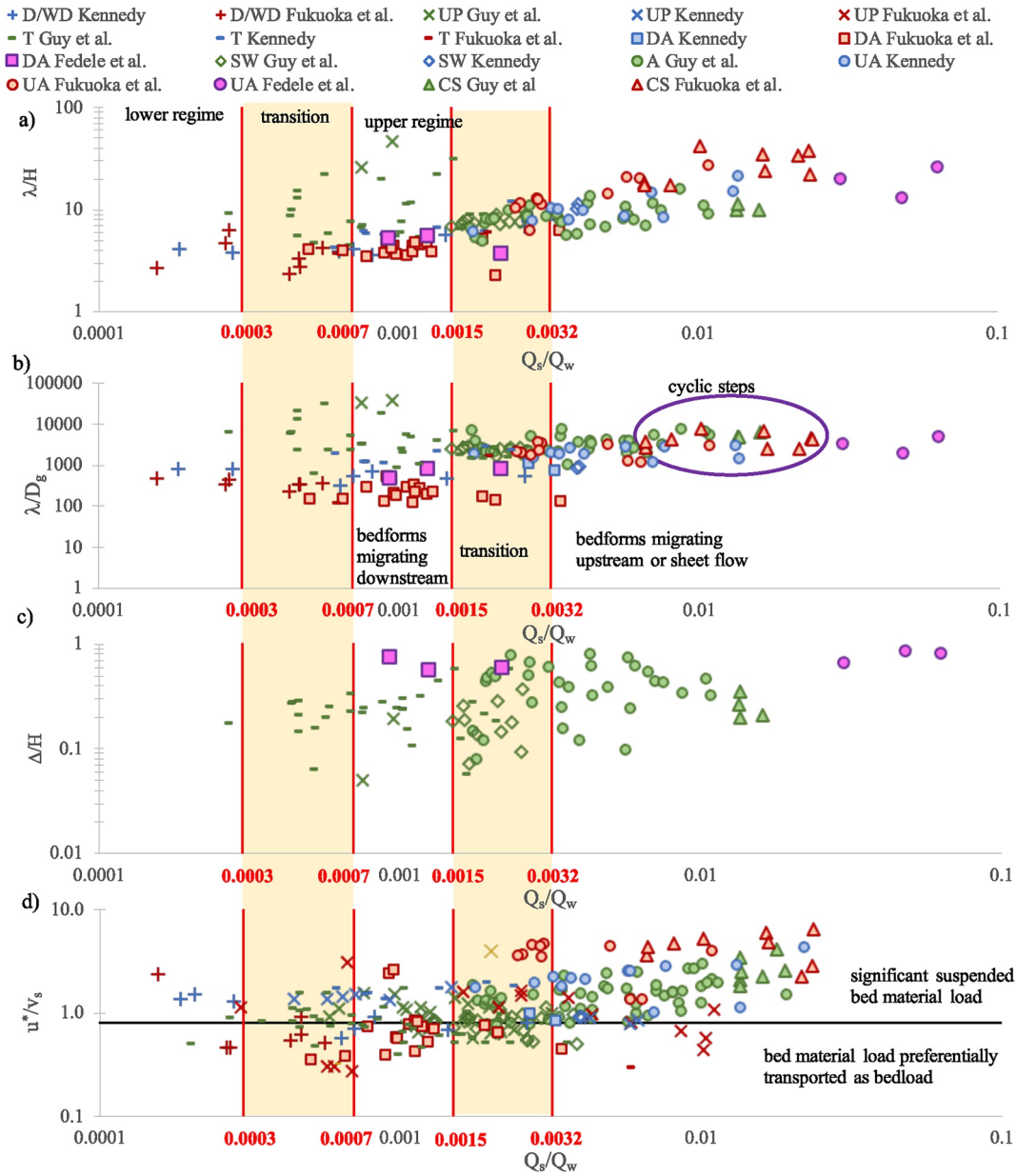

Figure 10. Data of experiments by Guy et al. (1966) (green), Kennedy (1961) (blue), Fukuoka et al. (1982) (red), and Fedele et al. (2016) (pink) in non-dimensional spaces of Figure 9. Line symbols denote lower regime bedforms, that is, dunes and washed out dunes D/WD, upper regime plane bed with a few grain diameters thick bedload layer UP and transitional states between bed configurations *T*. Shape symbols indicate upper regime bed configurations with open symbols indicating stationary bedforms, that is, standing waves (SW) SW, and filled symbols indicating migrating bedforms such as antidunes A (DA and UA respectively migrating downstream and upstream) and cyclic steps CS. Kennedy (1961) and Fukuoka et al. (1982) do not report measurements of bedform height. Guy et al. (1966) do not systematically report antidune migration direction, but their antidunes mostly migrate upstream.

as upstream migrating bedforms, 19 SW configurations of the 26 reported by Guy et al. (1966) are classified as transitional between upstream and downstream migrating bedforms. Only one downstream migrating antidune and two standing wave experiments by Kennedy (1961) and one downstream migrating antidune of the upper regime data by Fukuoka et al. (1982) were misclassified as upstream migrating bedforms. Further details are presented in the Table S1 in Supporting Information S1.

The classification of upper plane bed with few grain diameters thick bedload layer UP as typical of the transition zones of Figures 9 and 10 correctly predicts plane bed conditions for 47% of Guy et al. (1966) and Fukuoka

et al. (1982) experiments and for only 33% of the Kennedy experiment, suggesting that Q_s/Q_w is not a good predictor for upper plane bed configurations in the absence of bedload transport in sheet flow mode. As suggested by Naqshband, Ribberink, and Hulsher (2014) and Ohata et al. (2022), a predictor of the upper plane bed configuration UP should account for the presence of suspended bed material transport.

As observed in Figure 9, non-dimensional bedform length λ/H remains relatively constant and approximately equal to 3–5 for downstream migrating bedforms ($Q_s/Q_w < 0.0015$) and this is remarkably similar to the submarine case, where λ/H of most downstream-migrating antidunes reported by Fedele et al. (2009, 2016) (called in these studies "short" antidunes) is within the same range. Then, λ/H rapidly increases as the equilibrium configuration transitions to SW, upstream migrating antidunes, and cyclic steps (Figure 10a).

The gradual decrease in λ/D_g at the transition between the lower and upper regimes observed in Figure 9b is also present in Figure 10b (the scale of the vertical axis in Figure 10b is logarithmic). For $Q_s/Q_w > 0.0015$, the bedform height relative to water depth Δ/H increases with Q_s/Q_w. Heights of upstream migrating antidunes are greater than 60% of water depth (Figure 10c), as observed for the experiments with fine sand of Figure 9.

These trends are also noted for submarine cases although, as indicated in Fedele (2003), a characteristic imprint of the grain size effect is seen when looking at the bedform steepness, the ratio between bedform height to wavelength. In particular, for both downstream and upstream migrating equilibrium antidunes, the steepness (or "bumpiness") increases with grain size, suggesting effects of the importance of bedload to suspension in the mechanics of bedform formation, equilibrium and migration (Fedele, 2003; Fedele et al., 2016).

Finally, Figure 10d confirms that (a) suspended sand load ($u^*/v_s > 0.8$) occurred in experiments with upstream migrating bedforms (antidunes and cyclic steps), (b) downstream migrating antidunes formed with limited or negligible suspended load, and (c) upper plane bed conditions occurred with and without suspended sand transport. Interestingly, at values of Q_s/Q_w typical of upstream migrating bedforms ($Q_s/Q_w > 0.0032$), upper plane bed configurations occur with values of u^*/v_s close to or smaller than 0.8, indicating limited suspended sand load. The criterion $u^*/v_s > 0.8$ correctly predicts suspended load in 100 of the 113 experiments with significant suspension and in 57 of the 60 experiments with antidunes in the experiments by Guy et al. (1966) considered here.

6.2. Comparison With Other Non-Dimensional Parametric Spaces

Bedform classifications based on non-dimensional groups used in previous studies fail to capture either the progression from lower regime to upper regime bedforms, the progression from downstream migrating antidunes to upstream migrating antidunes or both. Data of Figure 9 are plotted against Froude number Fr and non-dimensional flow depth H/D with D denoting a characteristic sediment size (Vanoni, 1974) in Figures S1 and S2 in Supporting Information S1, ratio U/u^* (Engelund, 1966) in Figure S3 in Supporting Information S1, sidewall corrected Shields number $\tau_b^* = u^{*2}/RgD$ and Re_p (Ohata et al., 2017) in Figures S4 and S5 in Supporting Information S1. We also considered three parameters associated with skin friction to characterize the flow in the absence of bedforms (i.e., base flow of many analytical studies): the Froude number Fr_o, the ratio U/u_o^* and the Shields number τ_{bo}^*, results are in Figures S6–S8 in Supporting Information S1 respectively.

Classifications based on Froude number Fr and Fr_o capture the transition from lower to upper regime, as expected based on previous work by Engelund (1970) and Vanoni (1974) but fail to distinguish between downstream and upstream migrating bedforms. It is important to note that observations from large sand bed rivers such as the Mississippi River or Parana River show more complex transitions between large-scale dunes and flattening of those, for Froude numbers $Fr <<< 1$, thus much different from the transition values classically reported in the literature ($Fr \sim 1$) (but see Naqshband, Ribberink, & Hulsher, 2014).

The lower regime—upper regime transition for data of Figure 9 is characterized by values of Fr between 0.65 and 1 and Fr_o between 0.84 and 1.1. The comparison with the fluvial data of Figure 10 confirms that Fr-based criterion captures the lower regime—upper regime transition, given that most of these criteria were developed after these or similar studies from laboratory experiments. But it is important to note that this criterion does not allow any classification of upper regime bedform based on migration direction (Figure S9 in Supporting Information S1).

When a Froude number between 0.65 and 1 is used as a predictor of plane bed UP configurations, one of the four plane beds (25%) in Figure 9 is correctly classified. The same Fr-based criterion correctly classifies 71% of Guy

et al. (1966), 60% of Kennedy (1961) and 30% of Fukuoka et al. (1982) plane beds with a few grain-diameter-thick bedload layer indicating that other physical processes should be accounted for to adequately characterize the plane bed configuration (Ohata et al., 2022).

Classifications based on H/D and U/u^* do not capture bedform progression for the data of Figure 9 and for the fluvial data of Figure 10 (Figures S10 and S11 in Supporting Information S1). Classifications based on τ_b^* and τ_{bo}^* capture bedform progression from lower to upper regime with transitions for values of τ_b^* between 0.30 and 0.55 and of τ_{bo}^* between 0.25 and 0.30, but fail to reproduce the downstream migrating antidune—plane bed with bedload transport in sheet flow mode progression, as well as the transitions from upstream migrating antidune to breaking antidunes, that is, the bedform elongation toward the formation of cyclic steps.

7. Conclusions

Open channel flow experiments were conducted in a sediment feed flume to study the effect of sand supply rate and caliber on open-channel flow upper regime bedforms at equilibrium, that is, when the flow conditions and the bed configuration do not change in time. Data analysis and the comparison with previous experiments revealed that (a) parameters controlling the equilibrium state Q_w, Q_s and D_g (Blom et al., 2016 and references therein) expressed in terms of Q_s/Q_w play a prime control on equilibrium bed configuration in fine ($D_g < 0.5$ mm) and coarse sand, and (b) suspended sand load is critical for the formation of upstream migrating bedforms.

For values of Q_s/Q_w between 0.0003 and 0.0007, bedforms progress from washed-out dunes (lower regime) to downstream migrating antidunes (upper regime). This transition occurs with decreasing λ/D_g, constant values of λ/H and increasing Δ/H. At values of Q_s/Q_w greater than 0.0015, bedform length increases, which corresponds to a change in the bed configuration. For values of Q_s/Q_w greater than 0.0032, upstream migrating antidunes form in fine sand and progress to breaking antidunes and cyclic steps as Q_s/Q_w increases. These changes in bedform type are characterized by increasing values of λ/D_g, λ/H, and Δ/H. Bedform progression in coarse sand sees the development of upper plane bed with bedload transport in sheet flow mode and the formation of long wavelength and small amplitude bedforms (R. R. Hernandez Moreira et al., 2020). In other words, as downstream migrating antidunes progress into the plane bed in the presence of sheet flow, λ/D_g and λ/H increase and Δ/H decrease. An upper plane bed with a few grain diameters thick bedload layer was observed for a wide range of values of Q_s/Q_w. Standing waves tend to form when $0.0015 < Q_s/Q_w < 0.0032$ and downstream migrating antidunes progress into upstream migrating antidunes.

Data Availability Statement

The data set of all the experiments performed at the University of South Carolina are publicly available through the Dryad repository (R. Hernandez-Moreira, 2022; Jafarinik, 2022; Sanders, 2022).
Each data set contains Excel files with measurements of water surface and bed elevation, bedform geometry and migration rates and the hydraulic parameters used to characterize the flow and the bed configuration. Videos and pictures recorded during the runs as well as excel files containing information on velocity profiles, suspended sediment concentrations, instantaneous elevation of the channel bed and grain size of the emplaced deposits are available for selected experimental conditions.

Acknowledgments
The authors thank Gary Parker for translating relevant portions of the Fukuoka et al. (1982) paper and three anonymous reviewers whose criticisms helped improve the analysis. Sydney Sanders and Sadegh Jafarinik were supported with a grant from ExxonMobil. Ryan Johnson, Amanda Balkus, Mahsa Ahmadpoor, Brandon Fryson, and Briana McQueen were supported through the NSF award CBET 1751926 and REU supplements.

References

Alexander, J., Bridge, J. S., Cheel, R. J., & Leclair, S. F. (2001). Bedforms and associated sedimentary structures formed under supercritical water flows over aggrading sand beds. *Sedimentology*, *48*(1), 133–152. https://doi.org/10.1046/j.1365-3091.2001.00357.x

Andreotti, B., Claudin, P., Devaicjelle, O., Duran, O., & Fourriere, A. (2012). Bedforms in a turbulent stream: Ripples, chevrons and antidunes. *Journal of Fluid Mechanics*, *690*, 94–128. https://doi.org/10.1017/jfm.2011.386

Araya, T., & Masuda, F. (2001). Sedimentary structures of antidunes: An overview. *Journal of the Sedimentological Society of Japan*, *53*, 1–15. https://doi.org/10.4096/jssj1995.53.1

Bagnold, R. A. (1966). Sediment transport problem from general physics. In *Geological survey professional paper 422-I*. United States Printing Office.

Best, J. (2005). The fluid dynamics of river dunes: A review and some future research directions. *Journal of Geophysical Research*, *110*(F4), F04S02. https://doi.org/10.1029/2004jf000218

Best, J., & Bridge, J. (1992). The morphology and dynamics of low amplitude bedwaves upon upper stage plane beds and the preservation of planar laminae. *Sedimentology*, *39*(5), 737–752. https://doi.org/10.1111/j.1365-3091.1992.tb02150.x

Blom, A., Arkesteijn, L., Chavarrías, V., & Viparelli, E. (2017). The equilibrium alluvial river under variable flow and its channel-forming discharge. *Journal of Geophysical Research: Earth Surface*, *122*(10), 1924–1948. https://doi.org/10.1002/2017jf004213

Blom, A., Viparelli, E., & Chavarrías, V. (2016). The graded alluvial river: Profile concavity and downstream fining. *Geophysical Research Letters*, *43*(12), 6285–6293. https://doi.org/10.1002/2016gl068898

Bridge, J. S., & Best, J. L. (1988). Flow, sediment transport and bedform dynamics over the transition from dunes to upper-stage plane beds: Implications for the formation of planar laminae. *Sedimentology*, *35*(5), 753–763. https://doi.org/10.1111/j.1365-3091.1988.tb01249.x

Carling, P. A., & Shvidchenko, A. B. (2002). A consideration on the dune:antidune transition in fine gravel. *Sedimentology*, *49*(6), 1269–1282. https://doi.org/10.1046/j.1365-3091.2002.00496.x

Charru, F., Andreotti, B., & Claudin, O. (2013). Sand ripples and dunes. *Annual Review of Fluid Mechanics*, *45*(1), 469–493. https://doi.org/10.1146/annurev-fluid-011212-140806

Chiew, Y., & Parker, G. (1994). Incipient sediment motion on non-horizontal slopes. *Journal of Hydraulic Research*, *32*(5), 649–660. https://doi.org/10.1080/00221689409498706

Colombini, M. (2004). Revisiting the linear theory of sand dune formation. *Journal of Fluid Mechanics*, *502*, 1–16. https://doi.org/10.1017/s0022112003007201

Colombini, M., & Stocchino, A. (2008). Finite-amplitude river dunes. *Journal of Fluid Mechanics*, *611*, 283–396. https://doi.org/10.1017/s0022112008002814

Covault, J. A., Kostic, S., Paull, C. K., Sylvester, Z., & Fildani, A. (2017). Cyclic steps and related supercritical bedforms: Building blocks of deep-water depositional systems, western North America. *Marine Geology*, *393*, 4–20. https://doi.org/10.1016/j.margeo.2016.12.009

Einstein, H. A., & Barbarossa, N. L. (1952). River channel roughness. *Transactions of the American Society of Civil Engineers*, *117*(1), 1121–1146. https://doi.org/10.1061/taceat.0006666

Engelund, F. (1966). Hydraulic resistance of alluvial streams. *Journal of the Hydraulics Division, Proceedings of the American Society of Civil Engineers*, *92*(2), 315–326. https://doi.org/10.1061/jyceaj.0001417

Engelund, F. (1970). Instability of erodible beds. *Journal of Fluid Mechanics*, *42*(2), 225–244. https://doi.org/10.1017/s0022112070001210

Engelund, F., & Fredsoe, J. (1982). Sediment ripples and dunes. *Annual Review of Fluid Mechanics*, *14*(1), 13–37. https://doi.org/10.1146/annurev.fl.14.010182.000305

Engelund, F., & Hansen, E. (1967). *A monograph on sediment transport in alluvial streams*. Teknisk Forlag.

Fedele, J. J. (2003). *Bedforms and gravity underflows in marine environments. PhD Thesis*. University of Illinois at Urbana-Champaign.

Fedele, J. J., Guentzel, C., & Hoyal, D. (2009). Experiments on bedforms created by density currents. In *Proceedings 6th symposium on river coastal and estuarine morphodynamics RCEM, Santa Fe, Argentina*.

Fedele, J. J., Hoyal, D., Barnaal, Z., Tulenko, J., & Awalt, S. (2016). Bedforms created by gravity flows. In D. A. Budd, E. A. Hajek, & S. J. Purkis (Eds.), *Autogenic dynamics and self-organization in sedimentary systems* (Vol. 106, pp. 95–121). SEPM Special Publication.

Fredsoe, J. (1974). On the development of dunes in erodible channels. *Journal of Fluid Mechanics*, *64*(1), 1–16. https://doi.org/10.1017/s0022112074001960

Froude, M. J., Alexander, J., Barclay, J., & Cole, P. (2017). Interpreting flash flood paleoflow parameters from antidunes and gravel lenses: An example from Montserrat, West Indies. *Sedimentology*, *64*(7), 1817–1845. https://doi.org/10.1111/sed.12375

Fukuoka, S., Okutsu, K., & Yamasaka, M. (1982). Dynamic and kinematic features of sand waves in upper regime. *Proceeding of the Japan Society of Civil Engineering*, *323*, 77–89. (in Japanese). https://doi.org/10.2208/jscej1969.1982.323_77

Garcia, M. H. (1990). *Depositing and eroding sediment-driven flows: Turbidity currents. Project report 306*. St. Anthony Falls Laboratory, University of Minnesota.

Garcia, M. H. (2008). Sediment transport and morphodynamics. Chapter 2. In M. H. Garcia (Ed.), *Sedimentation engineering. Processes, measurements, modeling and practice, ASCE manuals and reports on engineering practice 110* (pp. 21–163). ASCE.

Guy, H. P., Simons, D. B., & Richardson, E. V. (1966). Summary of alluvial channel data from flume experiments, 1956–61. In *Geological survey professional paper 462-I. Washington D.C.*

Hayashi, T., & Ozaki, S. (1979). Alluvial bedform analysis I: Formation of alternating bars and braids. Chapter 7. In H. W. Shen & H. Kikkawa (Eds.), *Application of stochastic processes in sediment transport*. Water Resources Publications.

Hernandez-Moreira, R. (2022). Emplacement of massive deposits by sheet flow [Dataset]. Dryad. https://doi.org/10.5061/dryad.c59zw3r9b

Hernandez Moreira, R. R. (2016). *Deposits emplaced in upper regime*. PhD thesis. Univeristy of South Carolina at Columbia. Retrieved from https://scholarcommons.sc.edu/

Hernandez Moreira, R. R., Jafarinik, S., Sanders, S., Kendall, C. G. S. C., Parker, G., & Viparelli, E. (2020). Emplacement of massive deposits by sheet flow. *Sedimentology*, *67*(4), 1951–1972. https://doi.org/10.1111/sed.12689

Ikeda, S. (1984). Prediction of alternate bar wavelength and height. *Journal of Hydraulic Engineering*, *110*(4), 371–386. https://doi.org/10.1061/(asce)0733-9429(1984)110:4(371)

Jafarinik, S. (2022). Suspended and bedload transport in an open channel laboratory flume [Dataset]. Dryad. https://doi.org/10.5061/dryad.34tmpg4nk

Jafarinik, S., Hernandez Moreira, R., & Viparelli, E. (2019). Alluvial morphodynamics of bedrock reaches transporting mixed-size sand. Laboratory experiments. *Journal of Geophysical Research: Earth Surface*, *124*(12), 3067–3089. https://doi.org/10.1029/2019jf005058

Johnson, J. P. L. (2014). A surface roughness model for predicting alluvial cover and bed load transport rate in bedrock channels. *Journal of Geophysical Research: Earth Surface*, *119*(10), 2147–2173. https://doi.org/10.1002/2013jf003000

Kennedy, J. F. (1961). *Stationary waves and antidunes in alluvial channels. Report KH-R-2 W*. M. Keck Laboratory of Hydraulics and Water Resources Division of Engineering, California Institute of Technology.

Kostaschuk, R., Best, J., & Villard, P. V. (2010). The influence of dunes on mixing in a migrating salt-wedge: Fraser River estuary, Canada. *Earth Surface Processes and Landforms*, *35*, 460–465. https://doi.org/10.1002/esp.1928

Kostic, S. (2014). Upper flow regime bedforms on levees and continental slopes: Turbidity current flow dynamics in response to fine-grained sediment waves. *Geosphere*, *10*(6), 1094–1103. https://doi.org/10.1130/ges01015.1

Lang, J., Le Heron, D. P., van den Berg, J. H., & Winsemann, J. (2021). Bedforms and sedimentary structures related to supercritical flows in glacigenic settings. *Sedimentology*, *68*(4), 1539–1579. https://doi.org/10.1111/sed.12776

Mohrig, D., Whipple, K. X., Hondzo, M., Ellis, C., & Parker, G. (1998). Hydroplaning of subaqueous debris flows. *GSA Bulletin*, *110*(3), 387–394. https://doi.org/10.1130/0016-7606(1998)110<0387:hosdf>2.3.co;2

Muto, T., Yamagishi, C., Sekiguchi, T., Yokokawa, M., & Parker, G. (2012). The hydraulic autogenesis of distinct cyclicity in delta foreset bedding: Flume experiments. *Journal of Sedimentary Research*, *82*(7), 545–558. https://doi.org/10.2110/jsr.2012.49

Nakagawa, H., & Tsujimoto, T. (1980). Sand bed instability due to bedload motion. *Journal of the Hydraulics Division of the American Society of Civil Engineers*, *106*(12), 2029–2051. https://doi.org/10.1061/jyceaj.0005580

Naqshband, S., Hoitink, A. J. F., McElroy, B., Hurther, D., Ribberink, J. S., & Hulsher, S. J. M. H. (2017). A sharp view on river dune transition to upper stage plane bed. *Geophysical Research Letters*, *44*(22), 11437–11444. https://doi.org/10.1002/2017gl075906

Naqshband, S., Ribberink, J. S., & Hulsher, S. J. M. H. (2014). Using both free surface effect and sediment transport mode parameters in defining the morphology of river dunes and their evolution to upper stage plane beds. *Journal of Hydraulic Engineering*, 06014010.

Naqshband, S., Ribberink, J. S., Hurther, D., & Hulsher, S. J. M. H. (2014). Bed load and suspended load contributions to migrating sand dunes. *Journal of Geophysical Research: Earth Surface*, *119*(5), 1043–1063. https://doi.org/10.1002/2013jf003043

Nelson, J. M., Logan, B. L., Kinzel, P. J., Shimizu, Y., Giri, S., Shreve, R. L., & McLean, S. R. (2011). Bedform response to flow variability. *Earth Surface Processes and Landforms*, *36*(14), 1938–1947. https://doi.org/10.1002/esp.2212

Normark, W. R., Piper, D. J. W., Posamantier, H., Pirmez, C., & Migeon, S. (2002). Variability in form and growth of sediment waves on turbidite channel levees. *Marine Geology*, *192*(1–3), 23–58. https://doi.org/10.1016/s0025-3227(02)00548-0

Nunez-Gonzalez, F., & Martin-Vide, J. P. (2010). Downstream-migrating antidunes in sand, gravel and sand-gravel mixtures. In A. Dittrich, K. Koll, J. Aberle, & P. Geisenhainer (Eds.), *Proceedings of the international conference of fluvial hydraulics—River flow 2010* (pp. 393–400). Bundesanstalt für Wasserbau.

Ohata, K., Naruse, H., & Izumi, N. (2021). Linear stability analysis of plane beds under flows with suspended load. In *Earth surface dynamics discussion paper*. https://doi.org/10.5194/esurf-2021-60

Ohata, K., Naruse, H., & Izumi, N. (2022). Upper and lower plane bed definitions revised. *Progress in Earth and Planetary Science*, *9*(1), 23. https://doi.org/10.1186/s40645-022-00481-8

Ohata, K., Naruse, H., Yokokawa, M., & Viparelli, E. (2017). New bedform phase diagrams and discriminant functions for formative conditions of bedforms in open-channels. *Journal of Geophysical ResearchEarth Surface*, *122*(11), 2139–2158. https://doi.org/10.1002/2017jf004290

Paola, C., Wiele, S. M., & Reinhart, M. A. (1989). Upper-regime parallel lamination as the result of turbulent sediment transport and low-amplitude bed forms. *Sedimentology*, *36*(1), 47–59. https://doi.org/10.1111/j.1365-3091.1989.tb00819.x

Parkash, B., & Middleton, G. V. (1970). Downcurrent textural changes in Ordovician turbidite greywackes. *Sedimentology*, *14*(3–4), 259–293. https://doi.org/10.1111/j.1365-3091.1970.tb00195.x

Parker, G. (2004). 1D sediment transport morphodynamics with applications to rivers and turbidity currents. Retrieved from http://hydrolab.illinois.edu/people/parkerg/

Parker, G., Garcia, M. H., Fukushima, Y., & Yu, W. (1987). Experiments on turbidity currents over an erodible bed. *Journal of Hydraulic Research*, *25*(1), 123–147. https://doi.org/10.1080/00221688709499292

Parker, G., & Izumi, N. (2000). Purelu erosional cyclic and solitary steps created by flow over a cohesive bed. *Journal of Fluid Mechanics*, *419*, 203–238. https://doi.org/10.1017/s0022112000001403

Pen, S., Izumi, N., & Coutinho de Lima, A. (2018). Linear stability analysis of upper-regime bed waves including the effect of density stratification. *Journal of Japan Society of Civil Engineers Series B1 (Hydraulic Engineering)*, *74*(4), I_1099–I_1104.

Sanders, S. (2022). Influence of sand supply and grain size on upper regime bedforms [Dataset]. Dryad. https://doi.org/10.5061/dryad.tdz08kq2j

Seminara, G. (2010). Fluvial sedimentary patterns. *Annual Review of Fluid Mechanics*, *42*(1), 43–66. https://doi.org/10.1146/annurev-fluid-121108-145612

Sequeiros, O. E., Naruse, H., Endo, N., Garcia, M. H., & Parker, G. (2009). Experimental study on self-accelerating turbidity currents. *Journal of Geophysical Research*, *114*(C5), C05025. https://doi.org/10.1029/2008jc005149

Sequeiros, O. E., Spinewine, B., Beaubouef, R. T., Sun, T., Garcia, M. H., & Parker, G. (2010). Characteristics of velocity and excess density profiles of saline underflows and turbidity currents flowing over a mobile bed. *Journal of Hydraulic Engineering*, *7*(1), 412–433. https://doi.org/10.1061/(asce)hy.1943-7900.0000200

Simons, D. B., & Richardson, E. V. (1962). Roughness on depth-discharge relations in alluvial channels. In *Geological survey water-supply paper 1498-E*. United States Government Printing Office.

Simons, D. B., & Richardson, E. V. (1966). Resistance to flow in alluvial channels. In *Geological survey professional paper 422-J*. United States Government Printing Office.

Southard, J. B., & Boguchwal, L. A. (1990). Bed configurations in steady unidirectional water flows. Part 2. Synthesis of flume data. *Journal of Sedimentary Petrology*, *60*(5), 658–679. https://doi.org/10.1306/212f9241-2b24-11d7-8648000102c1865d

Spinewine, B., Sequeiros, O. E., Garcia, M. H., Beaubouef, R. T., Sun, T., Savoye, B., & Parker, G. (2009). Experiments on wedge-shaped deep sea sedimentary deposits in minibasins and/or on channel levees emplaced by turbidity currents. Part II. Morphodynamic evolution of the wedge and of the associated bedforms. *Journal of Sedimentary Research*, *79*(8), 608–628. https://doi.org/10.2110/jsr.2009.065

Sun, T., & Parker, G. (2005). Transportational cyclic steps created by flow over and erodible bed. Part 2. Theory and numerical simulations. *Journal of Hydraulic Research*, *43*(5), 502–514. https://doi.org/10.1080/00221680509500148

Taki, K., & Parker, G. (2005). Transportational cyclic steps created by flow over an erodible bed. Part 1. Experiments. *Journal of Hydraulic Research*, *43*(5), 488–501. https://doi.org/10.1080/00221680509500147

Task Force on Bed Forms in Alluvial Channels of the Committee on Sedimentation. (1966). Nomenclature for bed forms in alluvial channels. *Journal of the Hydraulics Division, Proceedings of the American Society of Civil Engineers*, *92*(3), 51–64. https://doi.org/10.1061/jyceaj.0001457

Toniolo, H., Parker, G., Voller, V., & Beaubouef, R. T. (2006). Depositional turbidity currents in diapiric minibasins on the continental slope: Experiments-numerical simulations and upscaling. *Journal of Sedimentary Research*, *76*(5), 798–818. https://doi.org/10.2110/jsr.2006.072

Vanoni, V. A. (1974). Factors determining bed forms of alluvial streams. *Journal of the Hydraulics Division, Proceedings of the American Society of Civil Engineers*, *100*(3), 363–377. https://doi.org/10.1061/jyceaj.0003906

Vanoni, V. A., & Brooks, N. H. (1957). *Laboratory studies of the roughness and suspended load of alluvial streams. Report E-68*. Sedimentation Laboratory, California Institute of Technology.

van Rijn, L. (1984). Sediment transport, Part III: Bed Forms and alluvial roughness. *Journal of Hydraulic Engineering*, *110*(12), 1733–1754. https://doi.org/10.1061/(asce)0733-9429(1984)110:12(1733)

Viparelli, E., & Eke, E. C. (2021). Equilibrium of self-formed, single thread, sand-bed rivers. *Geophysical Research Letters*, *48*(20), e2021GL094591. https://doi.org/10.1029/2021gl094591

Viparelli, E., Solari, L., & Hill, K. M. (2015). Downstream lightening and upward heavying: Experiments with sediments differing in density. *Sedimentology*, *62*(5), 1384–1407. https://doi.org/10.1111/sed.12187

Wilson, K. C. (1987). Analysis of bed-load motion at high shear stress. *Journal of Hydraulic Engineering*, *113*(1), 97–103. https://doi.org/10.1061/(asce)0733-9429(1987)113:1(97)

Wright, S., & Parker, G. (2004a). Density stratification effects in sand-bed rivers. *Journal of Hydraulic Engineering*, *130*(8), 783–795. https://doi.org/10.1061/(asce)0733-9429(2004)130:8(783)

Wright, S., & Parker, G. (2004b). Flow resistance and suspended load in sand-bed rivers: Simplified stratification model. *Journal of Hydraulic Engineering*, *130*(8), 796–805. https://doi.org/10.1061/(asce)0733-9429(2004)130:8(796)

Yokokawa, M., Hasegawa, K., Kanbayashi, S., & Endo, N. (2010). Formative conditions and sedimentary structures of sandy 3D antidunes: An application of the gravel step-pool model to fine-grained sand in an experimental flume. *Earth Surface Processes and Landforms*, *35*(14), 1720–1729. https://doi.org/10.1002/esp.2069

Yokokawa, M., Takahashi, Y., Yamamura, H., Kishima, Y., Parker, G., & Izumi, N. (2011). Phase diagram for antidunes and cyclic steps based on suspension index, non-dimensional Chezy resistance coefficient and Froude number. In *Proceedings of the 7th IAHR symposium on river, coastal and estuarine morphodynamics (RCEM 2011)* (pp. 1789–1794).